HHS Public Access

Author manuscript

Acta Biomater. Author manuscript; available in PMC 2023 February 01.

Published in final edited form as:

Acta Biomater. 2022 February ; 139: 91–104. doi:10.1016/j.actbio.2020.11.042.

Electrospun conductive nanofiber yarns for accelerating mesenchymal stem cells differentiation and maturation into Schwann cell-like cells under a combination of electrical stimulation and chemical induction

Shaohua Wu[1,2], **Ye Qi**[1], **Wen Shi**[2], **Mitchell Kuss**[2], **Shaojuan Chen**[1], **Bin Duan**[2,3,4,*]

[1]College of Textiles & Clothing, Qingdao University, Qingdao, China

[2]Mary & Dick Holland Regenerative Medicine Program and Division of Cardiology, Department of Internal Medicine, University of Nebraska Medical Center, Omaha, NE, USA

[3]Department of Surgery, College of Medicine, University of Nebraska Medical Center, Omaha, NE, USA

[4]Department of Mechanical and Materials Engineering, University of Nebraska-Lincoln, Lincoln, NE, USA

Abstract

Development of multifunctional tube-filling materials is required to improve the performances of the existing nerve guidance conduits (NGCs) in the repair of long-gap peripheral nerve (PN) injuries. In this study, composite nanofiber yarns (NYs) based on poly(p-dioxanone) (PPDO) biopolymer and different concentrations of carbon nanotubes (CNTs) were manufactured by utilizing a modified electrospinning apparatus. We confirmed the successful incorporation of CNTs into the PPDO nanofibers of as-fabricated composite NYs. The PPDO/CNT NYs exhibited similar morphology and structure in comparison with pure PPDO NYs. However, the PPDO/CNT NYs showed obviously enhanced mechanical properties and electrical conductivity compared to PPDO NYs. The biological tests revealed that the addition of CNTs had no negative effects on the cell growth, and proliferation of rabbit Schwann cells (rSCs), but it better maintained the phenotype of rSCs. We also demonstrated that the electrical stimulation (ES) significantly enhanced the differentiation capability of human adipose-derived mesenchymal stem cells (hADMSCs) into SC-like cells (SCLCs) on the PPDO/CNT NYs. More importantly, a unique combination of ES and chemical induction was found to further enhance the maturation of hADMSC-SCLCs on the PPDO/CNT NYs by notably upregulating the expression levels of SC myelination-associated gene markers and increasing the growth factor secretion. Overall, this study showed that our electrically conductive PPDO/CNT composite NYs could provide a

*Corresponding author: Dr. Bin Duan, bin.duan@unmc.edu; Phone: +1-(402) 559-9637.

The authors declare no competing financial interests.

beneficial microenvironment for various cell activities, making them an attractive candidate as NGC-infilling substrates for PN regeneration applications.

Graphical Abstract

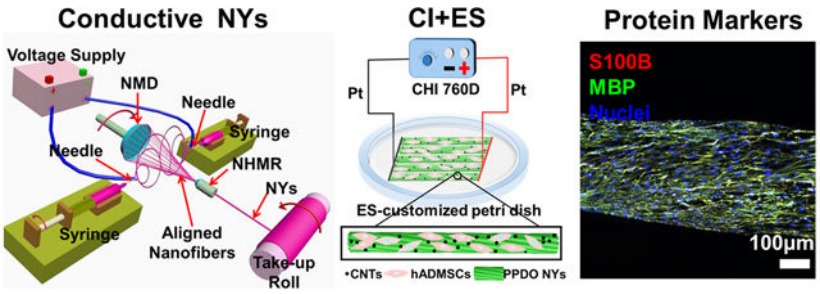

Keywords

electrospinning; electrical stimulation; cell differentiation; myelination; nerve regeneration

1. Introduction

Peripheral nerve injury (PNI) is a common clinical problem, which can disrupt the brain's communication with targeted muscles and organs, frequently leading to long-term impairment of motor and sensory functions and even life-long disability [1]. More than 550,000 patients require PNI treatments annually in the USA, with an enormous socioeconomic burden of approximately $1.6 billion [2]. In general, an end-to-end microsurgery is recognized as an effective therapeutic remedy for PNI with a defect gap less than 5 mm [3]. However, for severe PNI with a large gap (longer than 5 mm), the spontaneous regeneration from the human body is significantly restricted, and some form of graft is needed to bridge the nerve gap for promoting axonal regrowth and functional recovery [4]. Although there are many other grafts for the replacement therapy of severe PNI, such as allografts, xenografts, and man-made grafts, autologous grafts have been accepted as the gold standard substitute in clinics [5]. However, autografts still possess numerous inherent shortages, including limited donor supply, inaccurate sizes between donor nerve segment and the recipient site, and donor site morbidity [6]. In addition, many clinical reports have shown that although the autografts could promote the regeneration of damaged PN to some extent, the effective functional recovery remains insufficient and unsatisfactory, especially for severely-damaged PN [7]. In consequence, the repairing of severe PNI cases still represents a foremost challenge for clinical and translational neurosciences. The above-described situations have motivated the design and construction of alternative synthetic grafts, which could match or even surpass the performance of autografts [8].

With fantastic progress in regenerative medicine, especially in neuronal tissue engineering, various artificial and biological nerve grafts have been created in the past few decades [9, 10]. Many emerging studies indicated that the tissue engineered nerve grafts are promising and attractive substitutes to natural autografts [11, 12]. The nerve guidance

conduits (NGCs) with empty lumens have been considered as initial and basic structures for the construction of synthetic nerve grafts [13, 14]. Numerous clinical studies have demonstrated the effectiveness of single hollow NGCs. Moreover, some bioresorbable NGCs, such as type I collagen (Neuroflex™, NeuroMend™, Neuragen®) and poly(glycolic acid) (Neurotube®), have already been approved by US Food and Drug Administration (FDA) for human use[15]. Unfortunately, all of them are not recommended for a severe PNI with a gap over 3 cm. Existing studies indicated that the performances of synthetic NGCs are inferior to autologous grafts, probably because of the NGCs' lack of intraluminal ultrastructure and biological microenvironments, which could provide temporary support for guiding the regenerated nerve tissue to regrow from the proximal to distal ends [16, 17]. Many intraluminal filling materials, such as micro- or nano- fibers, hydrogels, and spongy matrix, have also been developed to modify the intratubal configurations of NGCs, but the outcomes thus far have been unsatisfactory [18, 19]. Based on the improved understanding of PN regeneration, an ideal design of intraluminal fillers should, firstly, better resemble the hierarchical ultrastructure and biological cues of a native PN system. Secondly, they should possess appropriate electrical properties, which are essential for the application of effective electrical stimulation (ES) during nerve regeneration. In addition, an appropriate selection of cell type and source is also a key factor for cellularizing NGC fillers, which notably influences the effectiveness of damaged PN regeneration.

The benefits of ES in promoting nerve regeneration and improving functional recovery of nerve injuries have been widely discussed and demonstrated in many previous studies[20, 21]. In the meanwhile, ES has already been successfully applied into some clinical treatments to remedy various neuronal disorders-related diseases, including depression, hearing loss, and Parkinson's disease [22, 23]. Some studies employed conductive polymers, including polyaniline (PANi), poly(3,4-ethylenedioxythiophene) (PEDOT), polypyrrole (PPy), and their derivatives, to improve the electrical conductivity of as-prepared nerve grafts. This technique has been demonstrated to enhance cell adhesion and neurite outgrowth both *in vitro* and *in vivo* [24, 25]. However, these conductive polymers have some limitations, such as apparently decreased conductivity in physiologic environments, brittleness, and poor processability [13]. In comparison, carbon nanotubes (CNTs) represent a new generation of conductive additives utilized for ES and recording in nerve tissue engineering [26]. CNTs are nanoscale in size and possess great conductivity, which make them an ideal candidate for a conductive filler for the construction of tissue engineered nerve constructs. Numerous studies demonstrated the feasibility of employing CNTs and biodegradable polymers in manufacturing a conductive composite for the repair and regeneration of damaged neural tissues [27, 28]. Additionally, several research groups have shown that exogenous ES through a conductive substance could motivate intracellular signaling pathways to promote neuroregeneration behaviors, such as neuronal outgrowth, cell differentiation, and synapse formation [29, 30].

In terms of cell sources utilized in PN tissue engineering, numerous different cell types have been explored. Among them, Schwann cells (SCs) and mesenchymal stem cells (MSCs) were the most widely employed[31]. SCs are the main glial cells in the PN system, which play an essential role in the reestablishment processes of injured PN, including secondary PN degeneration, axonal regrowth, and remyelination [32]. Unluckily, harvesting autologous

SCs is tremendously challenging due to their limited cell number and the high risk of donor site morbidity. Therefore, significant attention has been turned to the application of MSCs and several other types of stem cells [33–35]. Among different sources of MSCs, adipose derived MSCs (ADMSCs) have been widely explored to accelerate the damaged PN regeneration due to their clinical feasibility and relative ease of harvesting, expansion, and culturing[36]. Recent studies demonstrated that ADMSCs have a great capacity to differentiate into SC-like cells (SCLCs), which have similar function to native SCs to some extent [37–39]. However, effectively inducing and accelerating ADMSC differentiation and maturation towards SCs still remains a huge challenge. Our previous study showed that ADMSC derived SCLCs could express a high level of myelination-associated markers by the combinatorial use of appropriate culture matrix and chemical induction (CI) [40].

In the present study, we have designed and developed aligned nanofiber yarns (NYs) of CNT/poly(p-dioxanone) (PPDO) composite via a modified electrospinning approach, in order to confirm their biomimetic properties and to produce a simple but effective NGC intraluminal filler material for nerve tissue engineering. We hypothesized that the CNT/PPDO NYs could replicate the hierarchical and multiscale architecture of a native PN trunk to an extreme (in terms of size scale, topography, and structure). The incorporation of CNTs is expected to increase the electrical properties of PPDO NYs and have synergistic effects on PN regeneration once ES is applied. This study systematically investigated the cell morphology, growth, proliferation, and gene expression of rabbit SCs (rSCs) when seeded on various PPDO NYs and PPDO/CNT NYs. This study further compared the differentiation and maturation efficiency of human ADMSCs (hADMSCs) into SCLCs on CNT/PPDO NYs under CI, ES, and their combination.

2. Experimental

2.1 Preparation of PPDO NYs and PPDO/CNT NYs

PPDO NYs were manufactured by utilizing a modified electrospun nanofiber yarn-forming apparatus previously reported by our group (Figure 1A) [41]. In brief, PPDO (Mw=100,000, Corbion Purac, Netherlands) was dissolved in hexafluoro-2-propanol (HFIP, Acros Organics) to obtain a 10% (w/v) homogeneous solution. The PPDO solution was loaded into two syringes with 18-gauge blunt-pointed needles, which were placed opposite of each other at a distance of 20 cm. The solution flow rates in the two syringes were both controlled at the constant rate of 0.8 ml/h by two syringe pumps. A high voltage supply was utilized to apply positive and negative voltages of ±12 kV to the two needles, which could generate nanofibers with positive and negative charges, respectively. A neutral hollow metal rod (NHMR) and a neutral metal disc (NMD) were placed oppositely in the middle of the two needles, and the distance between the NMD and NHMR was set as 10 cm. The attractive nanofibers with different charges were collected between the NMD and NHMR. By anchoring the NHMR and rotating the NMD with a speed of 250 r/min, a stable spinning triangle cone was formed, which enabled the aligned nanofibers to be bundled into NYs. The obtained PPDO NYs were then guided to pass through the inner part of NHMR and be continuously collected on a rotating take-up roll. For the fabrication of CNT-loaded PPDO NYs, two different dosages (2 wt%, or 5 wt% relative to PPDO polymer) of CNTs

(multi-walled, 6–13 nm outer diameter, 2.5–20 μm length, Sigma) were dispersed in HFIP using an ultrasonic bath for 30 min. After that, PPDO pellets (10% (w/v) to HFIP) were added and stirred to generate CNT/PPDO suspensions (PPDO/2%CNT and PPDO/5%CNT). These suspensions were further electrospun to fabricate PPDO/2%CNT NYs and PPDO/5%CNT NYs on our electrospun nanofiber yarn-forming apparatus with the same processing variables as the fabrication of pure PPDO NYs. All of the as-obtained NYs were dried off by using a vacuum chamber before further utilization and characterization.

2.2 Physical and chemical characterizations of the NY materials

A scanning electron microscope (SEM, FEI Quanta 200) was employed to observe the morphologies of all of the NY specimens, i.e., PPDO NYs, PPDO/2%CNT NYs and PPDO/5%CNT NYs, after a gold coating process. The fiber orientation and the diameters of the obtained yarns and internal fibers were analyzed from the corresponding SEM images by Image J software (NIH). The dispersion of the CNTs in the PPDO nanofibers was confirmed by utilizing transmission electron microscopy (TEM, JEM-2100, JEOL). A Fourier transform infrared (FTIR) spectrometer (NEXUS-670, Nicolet) in attenuated total reflectance (ATR) mode was utilized to investigate the functional groups of all of the NY specimens. Raman spectra of the different NY samples were analyzed using a Micro-Raman spectrometer (LabRAM 800, Horiba Jobin-Yvon). The electrical conductivity of all the different NYs was determined by using a four-point probe testing unit (B2911A, Keysight Technologies). The mechanical properties of all the NY samples were characterized by using an Instron tensile testing machine. All of the tensile tests were performed with the same gauge length of 10 mm and a constant speed of 100 mm/min until failure occurred.

2.3 RSCs seeding and culture

The rSCs were isolated and derived from the sciatic nerve segments of three adult New Zealand white rabbits as reported by our previous studies [42]. The operations were carried out in accordance with the recommendations of the Guide for the Care and Use of Laboratory Animals from the National Research Council and the National Institutes of Health, and also in accordance with the Animal Welfare Act of the United States. The rSCs culture medium employed was Dulbecco's modified Eagle's medium (DMEM, Hyclone) supplemented with 10% fetal bovine serum (FBS, Gibco) and 1% penicillin/streptomycin (P/S, Invitrogen). The rSCs were utilized at passages 4–6. To investigate the effects of the PPDO/CNT composite on the cell behaviors, three different types of NYs (i.e., PPDO, PPDO/2%CNT, and PPDO/5%CNT) were utilized by fixing the ends of different 20mm length NY bundles with biological glue. Before rSC seeding, the NY bundles were sterilized in 70% ethanol overnight, and after washing them three times with sterilized phosphate buffered saline (PBS) solution, the bundles were pretreated with rSC culture medium overnight. After that, the rSCs, with a density of 5×10^4 cells per bundle, were seeded on the as-prepared NY bundles, cultured for 14 days, and characterized. The medium was changed every second day. All of the cell culture-related experiments in this study were carried out in an incubator with a humidified atmosphere of 5% CO_2 at 37 °C.

2.4 Electrical stimulation (ES) of rSCs

Several ES-customized petri dishes were employed to investigate the effects of ES on the cell behaviors of rSCs (Supplemental Figure S1). Two line-shaped platinum (Pt) electrodes were fixed onto the bottom of the petri dishes and were connected to the positive and negative poles of an electrochemical workstation (CHI 760D), respectively. The rSCs, with a density of 5×10^3 cells per cm^2, were seeded on the glass substrate and fixed in the middle of the two line-shaped Pt electrodes. The ES was conducted 1 h per day by using a mode of constant potential chronoamperometry with different potentials ranging from 0 to 500 mV/mm. The cellular activities of the rSCs were determined after 7 days of culture under ES.

2.5 HADMSCs seeding, culture, and differentiation

Primary hADMSCs were purchased from Lonza, USA and were utilized at passages 4–6. The hADMSC growth medium (GM) contained DMEM/F12 (Invitrogen), 10% FBS, and 1% P/S. Before cell seeding, PPDO/5%CNT NYs were cut into lengths of 25 mm and sterilized by using 70% ethanol overnight. After rinsing extensively with sterilized PBS, the sterilized PPDO/5%CNT NY samples were immersed completely in GM overnight. The hADMSCs were seeded on the pre-treated NY samples at a density of 5×10^3 cells per yarn. Three different types of induction methods, including CI, ES, and a combination of the two, were utilized to explore the differentiation capacity of hADMSCs towards matured SCLCs on the PPDO/5%CNT NYs (Figure 1B). For the CI process, a series of induction mediums (IM) were employed to culture the hADMSC-NY specimens according to our previously reported work. Firstly, the hADMSC-NY specimens were cultured in IM-(1), containing DMEM/F12, 1% P/S, and 1 mM β-mercaptoethanol (Sigma), for 24 h. After rinsing extensively with sterilized PBS, the medium was changed to IM-(2), containing DMEM/F12, 10% FBS, 1% P/S, and 35 ng/ml all trans-retinoic acid (Sigma), and cultured for 72 h. After rinsing extensively with sterilized PBS, the medium was replaced again with IM-(3), containing DMEM/F12, 10% FBS, 1% P/S, 5.7 μM forskolin (Sigma), 200 ng/ml recombinant human heregulin-β1 (PeproTech), 10 ng/ml basic fibroblast growth factor (bFGF, PeproTech), and 5 ng/ml recombinant human platelet derived growth factor-AA (PDGF-AA, PeproTech), and cultured for another 10 days. For ES treatment, a row of hADMSC-NY specimens were fixed onto the bottom of the ES-customized petri dishes. One end of the hADMSC-NY specimens was tightly contacted with the positive pole-connected Pt line electrode, and the other end was tightly contacted with the negative pole-connected Pt line electrode, which could make sure there were reliable and stable electrical connections on the whole hADMSC-NY specimens. The GM was employed for the cell culture, and the ES was performed 1 h per day from days 4 to 14 with a constant potential of 50 mV/mm. For the combination of CI and ES, the hADMSC-NY specimens were pre-treated by using IM-(1) for 24h and then induced by using IM-(2) for 72h. After that, IM-(3) and ES were simultaneously used for induction for another 10 days. The same ES parameters as the only ES treatment were utilized. For comparison, the hADMSCs on the PPDO/5%CNT NYs without CI and ES treatment were cultured in GM for 14 days, which was served as the control group. The cellular activities of hADMSCs in the four different groups were determined at the same time after 14 days of culture. The medium was changed with fresh medium on every second day of culture.

2.6 Cell viability and proliferation assay

The cell viability and morphology under different culture groups were characterized by utilizing a fluorescence-based Live/Dead viability/cytotoxicity assay (Invitrogen) similar to our previous reports [43, 44]. After 14 days of culture, cell-NY specimens were washed with warmed and sterilized PBS and further incubated with Calcein AM and EthD-1 containing medium. Stained samples were observed and imaged by using a confocal laser scanning microscope (CLSM, LSM 710, Carl Zeiss). The cell proliferation assays for different culture groups were carried out at day 7 and 14 by utilizing an MTT assay [45, 46].

2.7 Immunofluorescent (IF) staining

IF staining was conducted to determine the presence of SC-associated proteins in different cell culture groups. Briefly, after 14 days of culture, cell-seeded samples were washed three times in sterilized PBS to remove cell culture medium. Then the specimens were fixed in 4% paraformaldehyde for 4 h at 4 °C and were permeabilized by using 0.2% Triton X-100 for 10 min at room temperature after three times of PBS washing, and then were blocked in 1% BSA overnight at 4 °C after three times of PBS washing. The primary SC-specific antibodies, anti-S100B (1:250, Sigma) and anti- myelin basic protein (MBP) (1:200, Sigma), were employed to process the samples overnight at 4 °C. After washing three times with PBS the following day, samples were incubated with secondary fluorescent antibodies for 2 h at room temperature and then incubated with nuclear counterstaining (Draq 5, 1: 1000, Thermo Scientific) for 30 minutes at room temperature. Finally, the stained samples were washed one time with PBS and imaged with a Zeiss 710 CLSM.

2.8 RNA isolation and quantitative real-time PCR analysis

After 14 days of culture, QIA-Shredder and RNeasy mini-kits (QIAgen) were utilized to extract and purify the total RNA, according to the manufacturer's protocols. The obtained RNA was quantified at a 260 nm/280 nm absorbance ratio by using a NanodropTM OneC (Thermal Scientific). An iScript cDNA synthesis kit (BioRad Laboratories) was used to reverse transcribe RNA into cDNA. Quantitative real Time polymerase chain reaction (qRT-PCR) was carried out using SsoAdvanced SYBR Green Supermix (Bio-Rad) in a StepOne™ Real-Time PCR System (Thermo Scientific). Forty cycles were performed to analyze the target genes of interest, and 18S was used as the housekeeping gene. The ΔΔCt method was employed to determine the fold change analysis of each target gene. The sequences of primers, including S100B, glial fibrillary acidic protein (GFAP), sex determining region Y-box 10 (SOX10), nerve growth factor receptor (NGFR), neural cell adhesion molecule 1 (NCAM1), fatty acid binding protein 7 (FABP7), MBP, myelin protein zero (MPZ), and myelin-associated glycoprotein (MAG), were shown in Supplemental Table S1.

2.9 Human growth factor array assay

Three different types of induction methods, including CI, ES, and their combination, were utilized to treat hADMSCs, as described in section 2.8. In the meanwhile, hADMSCs cultured in GM were employed as the control group. On day 15, all of the media from the four different groups were collected and analyzed by utilizing a human growth factor array kit (RayBio® C-Series), according to the manufacturer's protocols. This kit could detect 41

different types of human growth factors, as shown in Supplemental Table S2. The arrays in each group were scanned, and signal intensities were quantified by using Image J software.

2.10 Statistical analysis

All the data were represented as mean ± standard deviation (SD) from at least three independent experiments. Comparison between pairwise groups was performed by using the one-way ANOVA with Scheffé post-hoc tests in statistical analysis. A difference of $p < 0.05$ was considered statistically significant.

3. Results

3.1 Morphological characterization of PPDO/CNT NYs

A modified electrospun nanofiber yarn-forming device (Figure 1A) was designed and implemented to manufacture PPDO NYs (Figure 2A) and two types of PPDO/CNT NYs, i.e., PPDO/2%CNT NYs (Figure 2B) and PPDO/5%CNT NYs (Figure 2C). SEM images showed that PPDO NYs without the addition of CNTs had highly aligned fibrous structures. Similarly, PPDO/2%CNT NYs and PPDO/5%CNT NYs also consisted of aligned bead-free nanofibers. The average yarn diameters of as-prepared PPDO NYs, PPDO/2%CNT NYs, and PPDO/5%CNT NYs were measured to be 216 ± 5, 215 ± 5, and 214 ± 5 μm, respectively (Supplemental Figure S2A), without statistical difference. Meanwhile, the diameters of the internal nanofibers of the three NY materials were also found to be comparable (483 ± 211 nm in the PPDO NYs vs. 468 ± 220 nm in the PPDO/2%CNT NYs vs. 443 ± 278 nm in the PPDO/5%CNT NYs) (Supplemental Figure S2B). The fiber orientation analysis showed that more than 70% of the nanofibers were highly aligned along the yarn's longitudinal direction for all the three types of PPDO NYs and PPDO/CNT NYs (within ±20°, Supplemental Figure S2C). TEM images revealed the obvious presence and location of CNTs within the PPDO nanofibers in both the PPDO/2%CNT NYs (Figure 2D) and PPDO/5%CNT NYs (Figure 2E). Taken together, these results confirmed that the addition of CNTs didn't significantly affect the morphology and structure of the as-obtained NY materials.

3.2 Raman spectra, FTIR spectra, and electrical conductivity of PPDO/CNT NYs

The Raman spectra were employed to further confirm the incorporation of CNTs into the PPDO nanofibers (Figure 2F). Both PPDO/2%CNT NYs and PPDO/5%CNT NYs exhibited two typical peaks for CNTs, i.e., D band (associated to sp^3 hybridization or other structural defects) at ~ 1333 cm^{-1} and G band (ascribed to sp^2 hybridization) at ~ 1593 cm^{-1}. As a comparison, no corresponding peaks were observed for PPDO NYs. We also calculated the intensity ratio of the D and G bands (I_D/I_G) to characterize the defects and disorder degree of CNTs in PPDO nanofibers. The I_D/I_G ratio was calculated to be 1.56 and 1.49 for PPDO/2%CNT NYs and PPDO/5%CNT NYs, respectively.

The chemical groups of PPDO NYs, PPDO/2%CNT NYs, and PPDO/5%CNT NYs were characterized by FTIR spectra (Figure 2G). For pure PPDO NYs, a sharp and narrow absorbance peak at ~1733 cm^{-1} was ascribed to the stretching vibration of C=O. The peak around 2917 cm^{-1} corresponded to a C-H stretching vibration. The peaks at ~1200 cm^{-1},

~1123 cm^{-1}, and ~1050 cm^{-1} are attributed to the stretching vibration of the C-O group. Moreover, the peak at ~1430 cm^{-1} was assigned to the bending vibrations of the CH_2 group. All of the characteristic peaks of PPDO polymer were also found in the PPDO/2%CNT NYs and PPDO/5%CNT NYs, and no obvious peak shifts were observed.

The electrical conductivities of the PPDO NYs, PPDO/2%CNT NYs, and PPDO/5%CNT NYs were determined to be 1.73×10^{-10}, 1.44×10^{-6}, and 3.52×10^{-6} $S \cdot cm^{-1}$, respectively (Figure 2H). It was found that the electrical conductivity of the PPDO/CNT NYs was dramatically enhanced due to the addition of CNTs, and the electrical conductivity of the PPDO/CNT NYs presented an increased trend with the increasing CNTs concentration.

3.3 Mechanical properties of PPDO/CNT NYs

The mechanical performances of the PPDO NYs and PPDO/CNT NYs were characterized by using tensile tests (Figure 3). The typical stress-strain curves showed that all of the NY samples presented a similar linear elastic behavior with subsequent plastic deformation until failure occurred (Figure 3A). Compared to pure PPDO NYs, both the PPDO/2%CNT NYs and PPDO/5%CNT NYs possessed notably enhanced Young's moduli (Figure 3B) and ultimate tensile strengths (Figure 3C) but lower ultimate strains. This demonstrated that the addition of CNTs increased the stiffness and strength of as-prepared NYs but also sacrificed the extensibility of the NYs to some extent, due to the high rigidity and high tensile strength of pristine CNTs. Moreover, we also found that the ultimate strength of the PPDO/CNT NYs was further increased with increasing the concentration of CNTs, whereas the ultimate strain decreased accordingly at higher concentration of CNTs.

3.4 PPDO/CNT NYs supported rSCs growth, and proliferation

RSCs were seeded on the PPDO NYs and PPDO/CNT NYs and cultured for 14 days to investigate the effects of NY components and morphology on cell behaviors. The cell morphology and viability are two important indicators in revealing the biocompatibility of a scaffold, which were visualized by utilizing a live/dead assay (Figure 4A). RSCs on all the three NY materials were found to possess high viability, with almost no dead cells being observed throughout 14 days of culture. We also found that the rSCs could sense the nanofibrous topography features and remodel their morphologies parallel to the alignment direction of nanofibers on all three NY materials (Figure 4A). The cell proliferation capability was evaluated by using an MTT assay (Figure 4B). The results showed that the number of rSCs on day 14 was significantly higher than those on day 7 when cultured on all three NY materials. The cell proliferation rate showed no significant differences among the three NY groups at each time point. These results indicated that the incorporation of CNTs, with a specific content, into PPDO nanofibers did not affect the cell viability and density throughout 14 days of culture, and all of the PPDO NYs and PPDO/CNT NYs provided a nanofibrous topography with high surface area, which were beneficial for not only supporting cell growth and proliferation, but also regulating the cell morphology by the contact guidance phenomenon.

3.5 PPDO/CNT NYs better supported the phenotype maintenance of rSCs

IF staining was employed to visualize the expression of SC-associated S100B protein when rSCs were seeded and cultured on the various PPDO NYs and PPDO/CNT NYs for 14 days (Figure 5A). S100B is one dominating marker expressed in most of the stages of SCs. The images showed that the rSCs cultured on all three of the NY materials were positively active in expressing S100B with strong green fluorescence, which seemingly had no significant differences among these three groups. The expression levels of several SC-related gene markers were quantified by qRT-PCR to further explore the phenotypic maintenance of rSCs when cultured on the different PPDO NYs and PPDO/CNT NYs for 14 days (Figure 5B). GFAP, SOX10, and NGFR are three early markers expressed by SC precursor cells or immature SCs. NCAM1 and FABP7 are two important markers expressed at the early stage of SC myelination. MBP and MPZ are three mature markers expressed at the late stage of SC myelination. The results showed that rSCs on the PPDO/5%CNT NYs presented significantly upregulated expression levels of S100B, GFAP, NGFR, MBP, and MPZ in comparison with those cultured on PPDO NYs and PPDO/2%CNT NYs, suggesting that the addition of CNTs was beneficial for the phenotypic maintenance of rSCs.

3.6 Appropriate ES treatment upregulated the expression of SC-specific gene markers of rSCs in 2D culture

We next explored the parameter-dependent effects of ES on the cell activities of rSCs. To simplify the research model, ES with different potentials (5, 50, 100, and 500 mV/mm) were applied to rSCs seeded on the 2D substrates for 1 h per day for 7 days. The images taken from an inverted optical microscope showed that when low ES potentials, ranging from 5 to 100 mV/mm, were adopted, rSCs cultured on the glass substrates presented high cell viability with normal cell morphologies at day 1, which are similar to those without ES treatment (Supplemental Figure S3). In comparison, obvious cell apoptosis/death was found in the group treated with a high ES potential of 500 mV/mm at day 1, suggesting that the high ES had negative effects on cell growth and proliferation. We also found that no significant differences in cell morphology and viability were shown in the groups without ES and with ES but using low potentials ranging from 5–100 mV/mm at day 7 (Figure 6A). The results from qRT-PCR analysis showed that rSCs exhibited significantly enhanced expression levels of S100B, GFAP, SOX10, FABP7, MBP, and MPZ genes in all three ES treated groups, compared to those in the group without ES (Figure 6B). No statistical differences were found for the expressions of S100B, SOX10, FABP7, MBP, and MPZ genes among the 5, 50, and 100 mV/mm treated groups and for the expression of the GFAP gene between the groups treated with 50 and 100 mV/mm. Taken together, these results demonstrated that an appropriate introduction of ES facilitated the phenotypic maintenance of rSCs in 2D culture.

3.7 A combination of ES and CI presented a synergistic effect on promoting the differentiation and maturation of hADMSCs towards myelinating SCLCs

As proved above, PPDO/5%CNT NYs not only possessed obviously enhanced electrical conductivity and mechanical properties, but they also presented improved biocompatibility by apparently enhancing the phenotypic maintenance of rSCs. In addition, PPDO/5%CNT

NYs supported hADMSC elongation and alignment (Supplemental Figure S4). Therefore, we selected them to further explore the effects of three different induction methods (i.e, chemical induction CI, ES, and a combination of ES and CI) on the differentiation and maturation of hADMSCs into SCLCs (Figure 1B). The corresponding groups were referred to as ES group, CI group, and ES+CI group. In comparison, hADMSCs seeded on PPDO/5%CNT NYs and cultured in GM were utilized as the control group, named as GM group. IF staining images showed that very limited expressions of both S100B (a marker expressed most stages of SCs) and MPB (a marker for mature SC) were detected in GM group (Figure 7A). However, hADMSCs cultured on PPDO/5%CNT NYs exhibited significantly enhanced expression of S100B in the CI group, ES group, and ES+CI group, while no differences were observed among these three groups. Interestingly, hADMSCs in CI group were weakly positive to the MBP staining, but enhanced expression of the MBP protein was found in the ES group compared to the GM and CI groups. Moreover, in comparison with the other three groups, the combination of CI and ES further increased the expression of MBP of hADMSCs in the group treated with both CI and ES.

QRT-PCR analysis was further utilized to determine the gene expression levels (Figure 7B). As expected, we found that the treatment of ES, CI, and their combination significantly upregulated the expression levels of S100B, GFAP, SOX10, FABP7, MBP, and MPG in hADMSCs compared to those in the GM group. In comparison with hADMSCs in the CI group, those in the ES group exhibited apparently robust expressions of S100B, GFAP, SOX10, FABP7, MAG, MBP, and MPG, suggesting that ES could notably improve the differentiation and maturation of hADMSCs to SCLCs, compared to CI. Importantly, the highest expression levels of S100B, MAG, and MBP genes were detected in the group with combined treatments, indicating that the combination of CI and ES could further enhance the maturation of hADMSC-SCLCs. Therefore, the synergistic effects of ES and CI made the hADMSCs-loaded PPDO/5%CNT NYs suitable for *in vivo* testing of PN regeneration applications.

3.8 A combination of CI and ES promoted the secretion of several growth factors of hADMSC-SCLCs

A human growth factor array was further employed to analyze the release behaviors of 41 different growth factors of hADMSC and hADMSC-SCLCs into the culture medium. The secretion of targeted growth factors was found in all the groups, including GM, ES, CI, and ES+CI groups (Figure 8). Compared to the ES group, the cells in CI group showed significantly higher levels of several interesting neurotrophic factors, including nerve growth factor (NGF), epidermal growth factor (EGF), and hepatocyte growth factor (HGF), which indicated that the CI treatment plays a more significant role on the production of neurotrophic factors than ES. We also found that ES and CI exhibited synergistic influences on the upregulated release of some growth factors, such as granulocyte colony-stimulating factor (GCSF) and insulin-like growth factor 1 receptor (IGF-1R), compared with CI treatment alone. Moreover, vascular endothelial growth factor-A (VEGF-A), an essential growth factor both promoting angiogenesis and nerve regeneration, was strongly detected in all the four groups, and no significant differences were found among the four

different groups. Taken together, the results suggested that a combination of ES and CI promoted growth factor secretion.

Discussion

Long-gap PN repair requires the development of an ideal graft or scaffold to provide a temporary support that regulates cellular behavior and promotes tissue regeneration [47]. Some previous studies have already demonstrated that the initial formation of aligned fibrin cables within the lumen of NGC, which bridge the disconnected proximal and distal stumps, is an essential factor concerning the whole PN regeneration process [48, 49]. Some other studies compared the differences of regeneration behavior between a slight PN crush injury and a severe PN transection injury [28, 50]. It was found that nerve fibers could be reconnected with 90% accuracy in a PN crush injury model, while the regeneration accuracy is significantly decreased in a PN transection injury due to the total loss of aligned nerve fibers and connective tissues. Therefore, it has become clear that one of the major limitations of single hollow NGCs is the lack of 3D intraluminal fillers, which can mimic the complex features of native extracellular matrix (ECM) of the PN stump.

In the present study, we designed and fabricated PPDO NYs and two types of conductive PPDO/CNT NYs (i.e., PPDO/2%CNT NYs and PPDO/5%CNT NYs) and systematically investigated their potentials for NGC-infilling material applications. Based on TEM images and Raman spectra analysis, we demonstrated the effective incorporation of CNTs into PPDO nanofibers in the PPDO/2%CNT NYs and PPDO/5%CNT NYs. SEM images and FTIR spectra analysis showed that the addition of CNTs didn’t obviously affect the size scale, structure, and chemical groups of as-fabricated PPDO/CNT NYs compared to the pure PPDO NYs. All three NYs had similar microscale diameters and contained highly aligned fibers with comparable nanoscale diameters. We implemented 2% and 5% CNTs because high CNT concentration was reported to have cytotoxicity [51, 52] and also affected the electrospinning process. It is known that the native PN stump consists of tightly packed aligned nerve fibers at the nanoscale level, which in turn organize to fascicles at the microscale level [4]. Therefore, our NYs could closely resemble the ultrastructure of nerve fibers and fascicles of native PN stump in terms of size scale, topography, and structure.

Besides appropriate topological and structural features, the NGC intraluminal filling materials must have sufficient mechanical properties, which could ensure the effective shape retention and stability during and after implantation [53, 54]. All of the as-developed NY materials in this work possessed great mechanical properties and structural integrity. Importantly, due to the inherent high rigidity and stiffness of CNTs, we found that when an appropriate amount of CNTs was embedded into PPDO nanofibers, it could obviously enhance the Young’s modulus and tensile strength of the finally-obtained NY materials. Other studies also demonstrated that a low amount of CNTs could be utilized to improve the mechanical properties of engineered grafts and scaffolds [55, 56]. PPDO polymer is one type of aliphatic polyester and widely employed to manufacture surgical synthetic absorbable monofilament sutures. The degradation behavior of PPDO is commonly composed with two stages [57, 58]. In the first stage (0–6 weeks), degradation takes place in the amorphous regions of PPDO leading to only minor weight loss. Then, in the second

stage (after 6 weeks), the crystallization regions of PPDO start to degrade, causing large weight loss. Moreover, PPDO has also been widely used to fabricate tissue-engineered scaffolds. Several previous studies reported that PPDO microfilaments were utilized as NGC-filling materials and found that PPDO microfilaments benefited the migration of host cells and promoted the axonal regeneration in the animal model [59, 60]. Several other studies employed PPDO as main materials to fabricate bio-absorbable conduits for nerve regeneration, and the degradation rate of the as-developed conduits could be controlled by the reasonable regulation of blending ratio of PPDO with other polymers [61, 62].

The ideal NGC fillers should have an appropriate electrical interaction with the neural and glial cells in order to enhance their biological functions. In order to replicate the electrical properties of the native PN stump, CNTs were employed as conductive additives to enhance the electrical conductivity of our NY materials. Due to the great conductivity of CNTs, it is no surprise to find that the conductivity of PPDO/CNT NYs significantly increased in comparison to the pure PPDO NYs. More specifically, the CNT-free PPDO NYs showed a conductivity value of 1.73×10^{-10} S·cm^{-1}, like an electrical insulator. The PPDO/2%CNT NYs and PPDO/5%CNT NYs incredibly increased the conductivity to be 1.44×10^{-6} and 3.52×10^{-6} S·cm^{-1}, respectively, which were roughly 1000 fold higher than that of the PPDO NYs. Other existing studies also demonstrated the feasibility of employing CNTs to enhance the conductivity of as-prepared grafts and scaffolds [63, 64].

The characteristics of a graft or scaffold, including size scale, topography, structure, and electrical conductivity, possess critical influences on cell behavior. In the present study, we first employed rSCs as model cells to characterize the biocompatibility and cytotoxicity of our PPDO NYs and PPDO/CNT NYs. SCs are considered significantly important for forming the bands of Büngner, and they support axonal regrowth and remyelination during PN regeneration. The biological results from the Live/Dead staining and MTT assay demonstrated that all three types of NYs not only supported cell growth and proliferation, but also effectively regulated the cell elongation and alignment by longitudinal contact guidance. As supported by previous reports, our results confirmed that the aligned polymeric fibers with apparently reduced diameters (100–1000 nm) can greatly enhance cell alignment, and proliferation [65, 66]. We also found that the CNTs in the PPDO/CNT NYs had no toxicity for rSCs, and no significant differences were found among the CNT-free PPDO NYs, PPDO/2%CNT NYs, and PPDO/5%CNT NYs in terms of cell viability and proliferation. It is worth noting that rSCs grown on PPDO/CNT NYs showed an obviously increased capability of phenotypic maintenance compared to those on CNT-free PPDO NYs. Some other studies have also suggested that the CNT-loaded biomaterials are capable of supporting the survival, growth, differentiation, and maturation of nerve-related cells, including SCs, cortical neurons, dorsal root ganglia, as well as the neuron-like SH-SY5Y and PC-12 cell lines [27, 67, 68]. Although the exact mechanisms of how the CNTs regulate the cellular activities are still not fully understood, some studies have disclosed that CNTs could activate multiple cellular signaling pathways (for instance, phospholipase C signaling pathway and extracellular signal-regulated kinase signaling pathway) by interacting with cells through cell-surface receptor proteins and cell-membrane ion channels[69, 70]. Some other studies demonstrated that the high electrical conductivity of CNTs could enhance the intercellular junction and promote the secretion of neurotrophic factors [26, 63]. Based on

these results and analysis, we selected PPDO/5%CNT NYs to move forward for further ES experiments.

It is well known that ES has significant influence on neural and glial cell behaviors. Numerous previous studies have employed a wide range of ES parameters, from direct current signals to alternating current ones, from single times of stimulation for several minutes or several hours to multiple times of stimulation for several days or even several weeks, and potentials varying from 1 to 750 mV/mm [71, 72]. In this study, rSCs cultured on 2D substrates were stimulated for 1 h per day throughout 7 days using potentials from 5–500 mV/mm. We found that a potential over a high amount, like 500 mV/mm, was harmful for the cell viability. It was also found that rSCs stimulated in 5 mV/mm, 50 mV/mm, 100 mV/mm conditions resulted in obviously upregulated SC-related gene expressions compared to the unstimulated cells. For most genes, including S100B, GFAP, SOX10, FABP7, MBP, and MPZ, there were no significant differences between the 50 mV/mm and 100 mV/mm stimulated groups, indicating that a plateau may be achieved with an increasing stimulation potential. Based on these results and analysis, we chose a fixed potential of 50 mV/mm for 1 h per day to move forward with further ES experiments.

The remyelination capacity of SCs is of critical importance for influencing the successful regeneration of injured PN tissue in the late stage. As one of the ideal cell types and sources, the effective induction and regulation of hADMSCs into myelinating SCLCs still remains a tremendous challenge in nerve tissue engineering. In the present study, we employed three methods, including ES, CI, and a combination of ES and CI, to investigate their effects on hADMSCs differentiation, maturity, and growth factor secretion. The results showed that CI could effectively regulate hADMSC differentiation into SCLCs on PPDO/5%CNT by significantly enhancing the expressions of several SC-related genes. Consistent with previous studies [73–75], we also confirmed that appropriate CI treatment could significantly enhance the release of neurotrophic factors of hADMSC-SCLCs. However, CI treatment alone, without ES, did not effectively induce hADMSC differentiation into SCLCs with a detectable expression of MBP on the PPDO/5%CNT NYs. Previous studies from our group and the other groups also demonstrated that a combinatorial use of CI and fibrous scaffolds could significantly improve the expressions of some early and immature SC markers of hADMSC-SCLCs, but not mature SC markers [40, 72, 76]. There are many existing studies demonstrating that a combination of the conductive substrates and ES synergistically enhanced the intercellular communication and promote various cell activities, including viability, adhesion, proliferation, and differentiation [77–81]. Based on our present study, we also found that ES significantly promoted further differentiation of hADMSCs into myelinating SCLCs, with higher expressions of the myelination-associated proteins (MBP) and genes (MBP, MAG, and MPZ) on conductive NYs compared to the CI and GM groups. Most importantly, ES synergized with CI to enhance hADMSCs differentiation towards myelinating hADMSC-SCLCs. For the first time, we demonstrated that a combination of ES and CI treatments improved the secretion of many growth factors of hADMSC-SCLCs that were essentially important for angiogenesis and nerve regeneration.

At the present stage, the mechanisms of the ES and CI combination treatments are unclear, and future studies should be conducted to better control and regulate the differentiation and

maturation of hADMSCs towards myelinating SCLCs. For instance, the existing studies showed that several signaling pathways, such as c-Jun and Raf/ERK, were involved in mediating the myelination of SCs *in vivo* [73, 82, 83], which may also play some roles on hADMSCs differentiation *in vitro*. One of the limitations of current study is that the myelination of axons for hADMSCs after CI and/or ES treatment is not verified. Future study will focus more on the co-culture of hADMSCs with either primary neurons from dorsal root ganglion or neuron cell lines with or without stimulation and identify the myelination capacities. Another limitation is that how electrical intensity affects hADMSC differentiation is not very clear. We have demonstrated that low ES potentials, ranging from 5 to 100 mV/mm, had no damage and positive effects on rSCs. The trend is supposed to be similar for hADMSC cultured on PPDO/CNT NYs. In addition, conventional electrodes were used in current study, which significantly induce high temperature due to the electrochemical reactions at the device/medium interface when high electrical potential and intensity was applied. This may be one of the results for damaging cells. In future study, some other novel electrical stimulation device, like hydrogel-based ion current-conducting circuit device [84, 85], could be used to safely apply higher intensity electrical stimulation and further study the effects on ADMSC differentiation. After we could control the differentiation status of ADMSCs (i.e. undifferentiation, differentiation to non-myelinating SCs, and differentiation to myelinating SCs), the further question will be how these differentiation status affect axon regenerations and remyelination *in vivo*. Clinically, it is envisioned that our PPDO/CNT NYs with or without ADMSCs could be effectively utilized as a promising NGC-infilling candidate for long-gap PN regeneration application.

Conclusions

In the present study, we incorporated a varied amount of CNTs into PPDO nanofibers to develop composite NYs by using a modified electrospinning method. The PPDO/CNT NYs exhibited some significantly different performances in comparison with the CNT-free PPDO NYs, such as improved mechanical properties and increased electrical conductivity. Moreover, the PPDO/CNT NYs also presented an obviously enhanced biocompatibility by effectively maintaining the phenotype of rSCs. In addition, by using PPDO/CNT NYs as cell carriers, CI was demonstrated to promote the SC-related growth factor secretion of hADMSCs, and ES was demonstrated to improve the phenotypic maturation of hADMSCs into myelinating SCLCs. Moreover, a unique combination of ES and CI was found to further synergistically enhance the maturation of hADMSC-SCLCs on the PPDO/CNT NYs. These results demonstrated that our electrically conductive PPDO/CNT NYs presented in this study support the cellular activities that are essential for PN regeneration, eventually making them an attractive candidate as NGC-intraluminal filling material.

Supplementary Material

Refer to Web version on PubMed Central for supplementary material.

Acknowledgements

This work has been supported by Mary & Dick Holland Regenerative Medicine Program start-up grant, Nebraska Research Initiative funding, National Institutes of Health (R01 AR073225), and Nebraska Stem Cell Research Project Grant. The authors would like to thank the financial support from National Key Research and Development Program of China (Grant no. 2017YFB0309805-2), and the Shandong Provincial Key Research and Development Program, China (Grant no. 2018GGX108003). The authors also would like to thank Tom Bargar and Nicholas Conoan of the Electron Microscopy Core Facility (EMCF) at the University of Nebraska Medical Center for technical assistance. The EMCF is supported by state funds from the Nebraska Research Initiative (NRI) and the University of Nebraska Foundation and institutionally by the Office of the Vice Chancellor for Research.

References

[1]. Vijayavenkataraman S, Nerve guide conduits for peripheral nerve injury repair: A review on design, materials and fabrication methods, Acta Biomaterialia 106 (2020) 54–69. [PubMed: 32044456]

[2]. Huang L, Zhu L, Shi X, Xia B, Liu Z, Zhu S, Yang Y, Ma T, Cheng P, Luo K, Huang J, Luo Z, A compound scaffold with uniform longitudinally oriented guidance cues and a porous sheath promotes peripheral nerve regeneration in vivo, Acta Biomaterialia 68 (2018) 223–236. [PubMed: 29274478]

[3]. Howarth HM, Orozco E, Lovering RM, Shah SB, A comparative assessment of lengthening followed by end-to-end repair and isograft repair of chronically injured peripheral nerves, Experimental neurology 331 (2020) 113328–113328. [PubMed: 32333909]

[4]. Tajdaran K, Chan K, Gordon T, Borschel GH, Matrices, scaffolds, and carriers for protein and molecule delivery in peripheral nerve regeneration, Experimental Neurology 319 (2019).

[5]. Cheng Z, Shen Y, Qian T, Yi S, He J, Protein phosphorylation profiling of peripheral nerve regeneration after autologous nerve grafting, Molecular and Cellular Biochemistry (2020).

[6]. Chrzaszcz P, Derbisz K, Suszynski K, Miodonski J, Trybulski R, Lewin-Kowalik J, Marcol W, Application of peripheral nerve conduits in clinical practice: A literature review, Neurologia I Neurochirurgia Polska 52(4) (2018) 427–435. [PubMed: 30025722]

[7]. Patel NP, Lyon KA, Huang JH, An update-tissue engineered nerve grafts for the repair of peripheral nerve injuries, Neural Regeneration Research 13(5) (2018) 764–774. [PubMed: 29862995]

[8]. Chen A, Lai X, Liang H, Zhang Y, Kang Y, Lin Y, Shao L, Nanoscaffolds in promoting regeneration of the peripheral nervous system, Nanomedicine 13(9) (2018) 1067–1085. [PubMed: 29790811]

[9]. Bu Y, Wang X, Li L, Hu X, Tan D, Li Z, Lai M, Qiu X, Sun F, Wang H, Yang F, Wu D, Guo J, Lithium Loaded Octa-Poly(Ethylene Glycol) Based Adhesive Facilitates Axon Regeneration and Reconnection of Transected Peripheral Nerves, Advanced Healthcare Materials (2020).

[10]. Jain D, Mattiassi S, Goh EL, Yim EKF, Extracellular matrix and biomimetic engineering microenvironment for neuronal differentiation, Neural Regeneration Research 15(4) (2020) 573–585. [PubMed: 31638079]

[11]. Regas I, Loisel F, Haight H, Menu G, Obert L, Pluvy I, Functionalized nerve conduits for peripheral nerve regeneration: A literature review, Hand surgery & rehabilitation (2020).

[12]. Brito A.C.N.d.L., Santos SEV, Martins WA, Queiroz P.C.d.S., Sougey WWD, Alves PKN, Ribeiro KL, de Oliveira MDL, de Moraes SRA, Efficacy of tubing technique with biomaterials compared to direct coaptation technique after peripheral neurotmesis in nerve healing and return to functionality in young adult rats: a systematic review protocol, Systematic Reviews 9(1) (2020).

[13]. Liu Y, Hsu S.-h., Biomaterials and neural regeneration, Neural Regeneration Research 15(7) (2020) 1243–1244. [PubMed: 31960803]

[14]. Uranues S, Bretthauer G, Tomasch G, Rafolt D, Nagele-Moser D, Berghold A, Kleinert R, Justich I, Waldert J, Koch H, A New Synthetic Conduit for the Treatment of Peripheral Nerve Injuries, World Journal of Surgery (2020).

[15]. Muheremu A, Ao Q, Past, Present, and Future of Nerve Conduits in the Treatment of Peripheral Nerve Injury, Biomed Research International (2015).

[16]. Li G, Zhao X, Zhang L, Yang J, Cui W, Yang Y, Zhang H, Anisotropic ridge/groove microstructure for regulating morphology and biological function of Schwann cells, Applied Materials Today 18 (2020).

[17]. Belanger K, Dinis TM, Taourirt S, Vidal G, Kaplan DL, Egles C, Recent Strategies in Tissue Engineering for Guided Peripheral Nerve Regeneration, Macromolecular Bioscience 16(4) (2016) 472–481. [PubMed: 26748820]

[18]. Cao Z, Yao S, Xiong Y, Zhang Z, Yang Y, He F, Zhao H, Guo Y, Wang G, Xie S, Guo H, Wang X, Directional axonal regrowth induced by an aligned fibrin nanofiber hydrogel contributes to improved motor function recovery in canine L2 spinal cord injury, Journal of Materials Science-Materials in Medicine 31(5) (2020).

[19]. Hou Y, Wang X, Zhang Z, Luo J, Cai Z, Wang Y, Li Y, Repairing Transected Peripheral Nerve Using a Biomimetic Nerve Guidance Conduit Containing Intraluminal Sponge Fillers, Advanced Healthcare Materials 8(21) (2019).

[20]. Zhao Y, Liang Y, Ding S, Zhang K, Mao H-Q, Yang Y, Application of conductive PPy/SF composite scaffold and electrical stimulation for neural tissue engineering, Biomaterials 255 (2020) 120164–120164. [PubMed: 32554132]

[21]. Hu X, Wang X, Xu Y, Li L, Liu J, He Y, Zou Y, Yu L, Qiu X, Guo J, Electric Conductivity on Aligned Nanofibers Facilitates the Transdifferentiation of Mesenchymal Stem Cells into Schwann Cells and Regeneration of Injured Peripheral Nerve, Advanced Healthcare Materials (2020).

[22]. Power HA, Morhart MJ, Olson JL, Chan KM, Postsurgical Electrical Stimulation Enhances Recovery Following Surgery for Severe Cubital Tunnel Syndrome: A Double-Blind Randomized Controlled Trial, Neurosurgery 86(6) (2020) 769–777. [PubMed: 31432080]

[23]. Gunter C, Delbeke J, Ortiz-Catalan M, Correction to: Safety of long-term electrical peripheral nerve stimulation: review of the state of the art, Journal of neuroengineering and rehabilitation 17(1) (2020) 77–77. [PubMed: 32539841]

[24]. Li Y, Huang Z, Pu X, Chen X, Yin G, Wang Y, Miao D, Fan J, Mu J, Polydopamine/carboxylic graphene oxide-composited polypyrrole films for promoting adhesion and alignment of Schwann cells, Colloids and Surfaces B-Biointerfaces 191 (2020).

[25]. Fan L, Xiong Y, Fu Z, Xu D, Wang L, Chen Y, Xia H, Peng N, Ye S, Wang Y, Zhang L, Ye Q, Polyaniline promotes peripheral nerve regeneration by enhancement of the brain-derived neurotrophic factor and ciliary neurotrophic factor expression and activation of the ERK1/2/MAPK signaling pathway, Molecular Medicine Reports 16(5) (2017) 7534–7540. [PubMed: 28944860]

[26]. Sun Y, Liu X, George MN, Park S, Gaihre B, Terzic A, Lu L, Enhanced Nerve Cell Proliferation and Differentiation on Electrically Conductive Scaffolds Embedded with Graphene and Carbon Nanotubes, Journal of biomedical materials research. Part A (2020).

[27]. Jahromi HK, Farzin A, Hasanzadeh E, Barough SE, Mahmoodi N, Najafabadi MRH, Farahani MS, Mansoori K, Shirian S, Ai J, Enhanced sciatic nerve regeneration by poly-L-lactic acid/multi-wall carbon nanotube neural guidance conduit containing Schwann cells and curcumin encapsulated chitosan nanoparticles in rat, Materials Science & Engineering C-Materials for Biological Applications 109 (2020).

[28]. Oprych KM, Whitby RLD, Mikhalovsky SV, Tomlins P, Adu J, Repairing Peripheral Nerves: Is there a Role for Carbon Nanotubes?, Advanced Healthcare Materials 5(11) (2016) 1253–1271. [PubMed: 27027923]

[29]. Liu Z, Yushan M, Alike Y, Liu Y, Wu S, Ma C, Yusufu A, Preparation of Multiwall Carbon Nanotubes Embedded Electroconductive Multi-Microchannel Scaffolds for Neuron Growth under Electrical Stimulation, Biomed Research International 2020 (2020).

[30]. Song S, George PM, Conductive polymer scaffolds to improve neural recovery, Neural Regeneration Research 12(12) (2017) 1976–1978. [PubMed: 29323032]

[31]. Liang Z, Lu L, Yu X, Study Brain Derived Neurotrophic Factor Gene Modified Schwann Cells Combined Chitosan Materials Treatment Peripheral Nerve Injury, Journal of Nanoscience and Nanotechnology 20(10) (2020) 6103–6110. [PubMed: 32384958]

[32]. Nocera G, Jacob C, Mechanisms of Schwann cell plasticity involved in peripheral nerve repair after injury, Cellular and molecular life sciences : CMLS (2020).

[33]. Yang Z, Zheng C, Zhang F, Lin B, Cao M, Tian X, Zhang J, Zhang X, Shen J, Magnetic resonance imaging of enhanced nerve repair with mesenchymal stem cells combined with microenvironment immunomodulation in neurotmesis, Muscle & Nerve 61(6) (2020) 815–825. [PubMed: 32170960]

[34]. Xu Z, Chen Z, Feng W, Huang M, Yang X, Qi Z, Grafted muscle-derived stem cells promote the therapeutic efficiency of epimysium conduits in mice with peripheral nerve gap injury, Artificial Organs 44(5) (2020) E214–E225. [PubMed: 31792982]

[35]. Bojanic C, To K, Zhang B, Mak C, Khan WS, Human umbilical cord derived mesenchymal stem cells in peripheral nerve regeneration, World Journal of Stem Cells 12(4) (2020) 288–302. [PubMed: 32399137]

[36]. Zhou LN, Wang JC, Zilundu PLM, Wang YQ, Guo WP, Zhang SX, Luo H, Zhou JH, Deng RD, Chen DF, A comparison of the use of adipose-derived and bone marrow-derived stem cells for peripheral nerve regeneration in vitro and in vivo, Stem Cell Research & Therapy 11(1) (2020).

[37]. Yamamoto D, Tada K, Suganuma S, Hayashi K, Nakajima T, Nakada M, Matsuta M, Tsuchiya H, Differentiated adipose-derived stem cells promote peripheral nerve regeneration, Muscle & Nerve (2020).

[38]. Fu X.-m., Wang Y, Fu W.-l., Liu D.-h., Zhang C.-y., Wang Q.-l., Tong X.-j., The Combination of Adipose-derived Schwann-like Cells and Acellular Nerve Allografts Promotes Sciatic Nerve Regeneration and Repair through the JAK2/STAT3 Signaling Pathway in Rats, Neuroscience 422 (2019) 134–145. [PubMed: 31682951]

[39]. Liu Y, Dong R, Zhang C, Yang Y, Xu Y, Wang H, Zhang M, Zhu J, Wang Y, Sun Y, Zhang Z, Therapeutic effects of nerve leachate-treated adipose-derived mesenchymal stem cells on rat sciatic nerve injury, Experimental and Therapeutic Medicine 19(1) (2020) 223–231. [PubMed: 31853293]

[40]. Wu S, Ni S, Jiang X, Kuss MA, Wang H-J, Duan B, Guiding Mesenchymal Stem Cells into Myelinating Schwann Cell-Like Phenotypes by Using Electrospun Core-Sheath Nanoyarns, Acs Biomaterials Science & Engineering 5(10) (2019) 5284–5294. [PubMed: 33455233]

[41]. Wu S, Duan B, Liu P, Zhang C, Qin X, Butcher JT, Fabrication of Aligned Nanofiber Polymer Yarn Networks for Anisotropic Soft Tissue Scaffolds, Acs Applied Materials & Interfaces 8(26) (2016) 16950–16960. [PubMed: 27304080]

[42]. Wu S, Kuss MA, Qi D, Hong J, Duan B, Development of Cryogel-based Guidance Conduit for Peripheral Nerve Regeneration, ACS Applied Bio Materials 2(11) (2019) 4864–4871.

[43]. Wu S, Wang Y, Streubel PN, Duan B, Living nanofiber yarn-based woven biotextiles for tendon tissue engineering using cell tri-culture and mechanical stimulation, Acta Biomaterialia 62 (2017) 102–115. [PubMed: 28864251]

[44]. Wu S, Peng H, Li X, Streubel PN, Liu Y, Duan B, Effect of scaffold morphology and cell co-culture on tenogenic differentiation of HADMSC on centrifugal melt electrospun poly (L-lactic acid) fibrous meshes, Biofabrication 9(4) (2017).

[45]. Wu S, Zhou R, Zhou F, Streubel PN, Chen S, Duan B, Electrospun thymosin Beta-4 loaded PLGA/PLA nanofiber/microfiber hybrid yarns for tendon tissue engineering application, Materials Science & Engineering C-Materials for Biological Applications 106 (2020).

[46]. Wei L, Wu S, Shi W, Aldrich AL, Kielian T, Carlson MA, Sun R, Qin X, Duan B, Large-Scale and Rapid Preparation of Nanofibrous Meshes and Their Application for Drug-Loaded Multilayer Mucoadhesive Patch Fabrication for Mouth Ulcer Treatment, Acs Applied Materials & Interfaces 11(32) (2019) 28740–28751. [PubMed: 31334627]

[47]. Chiono V, Tonda-Turo C, Trends in the design of nerve guidance channels in peripheral nerve tissue engineering, Progress in neurobiology 131 (2015) 87–104. [PubMed: 26093353]

[48]. Zhang X, Qu W, Li D, Shi K, Li R, Han Y, Jin E, Ding J, Chen X, Functional Polymer-Based Nerve Guide Conduits to Promote Peripheral Nerve Regeneration, Advanced Materials Interfaces (2020).

[49]. Du J, Liu J, Yao S, Mao H, Peng J, Sun X, Cao Z, Yang Y, Xiao B, Wang Y, Tang P, Wang X, Prompt peripheral nerve regeneration induced by a hierarchically aligned fibrin nanofiber hydrogel, Acta Biomaterialia 55 (2017) 296–309. [PubMed: 28412554]

[50]. Mok A, Allen J, Haney MM, Deninger I, Ballenger B, Caywood V, Osman KL, Zitsch B, Hopewell BL, Thiessen A, Szewczyk M, Ohlhausen D, Newberry CI, Leary E, Lever TE, A Surgical Mouse Model for Advancing Laryngeal Nerve Regeneration Strategies, Dysphagia 35(3) (2020) 419–437. [PubMed: 31388736]

[51]. Foldbjerg R, Irving ES, Wang J, Thorsen K, Sutherland DS, Autrupa H, Beer C, The toxic effects of single-walled carbon nanotubes are linked to the phagocytic ability of cells, Toxicology Research 3(4) (2014) 228–241.

[52]. Singhai NJ, Ramteke S, Functionalized Carbon Nanotubes: Emerging Applications in the Diverse Biomedical Arena, Current Nanoscience 16(2) (2020) 170–186.

[53]. Sensharma P, Madhumathi G, Jayant RD, Jaiswal AK, Biomaterials and cells for neural tissue engineering: Current choices, Materials Science & Engineering C-Materials for Biological Applications 77 (2017) 1302–1315.

[54]. Gu X, Ding F, Williams DF, Neural tissue engineering options for peripheral nerve regeneration, Biomaterials 35(24) (2014) 6143–6156. [PubMed: 24818883]

[55]. Steel EM, Azar J-Y, Sundararaghavan HG, Electrospun hyaluronic acid-carbon nanotube nanofibers for neural engineering, Materialia 9 (2020).

[56]. Zarei M, Karbasi S, Evaluation of the effects of multiwalled carbon nanotubes on electrospun poly(3-hydroxybutirate) scaffold for tissue engineering applications, Journal of Porous Materials 25(1) (2018) 259–272.

[57]. Dang H-C, Luo Y-K, Xu C, Song F, Wang X-L, Wang Y-Z, Contribution of Hemispheric CaCO3 To Improving Crystalline, Physical Properties and Biocompatibility of Poly(p-dioxanone), Industrial & Engineering Chemistry Research 54(24) (2015) 6269–6281.

[58]. Sabino MA, Albuerne J, Muller AJ, Brisson J, Prud'homme RE, Influence of in vitro hydrolytic degradation on the morphology and crystallization behavior of poly(p-dioxanone), Biomacromolecules 5(2) (2004) 358–370. [PubMed: 15002995]

[59]. Novikova LN, Kolar MK, Kingham PJ, Ullrich A, Oberhoffner S, Renardy M, Doser M, Mueller E, Wiberg M, Novikov LN, Trimethylene carbonate-caprolactone conduit with poly-p-dioxanone microfilaments to promote regeneration after spinal cord injury, Acta Biomaterialia 66 (2018) 177–191. [PubMed: 29174588]

[60]. Hoffmann N, Mittnacht U, Hartmann H, Baumer Y, Kjems J, Oberhoffner S, Schlosshauer B, Neuronal and glial responses to siRNA-coated nerve guide implants in vitro, Neuroscience Letters 494(1) (2011) 14–18. [PubMed: 21352894]

[61]. Wan Y, Zhang J, Luo Y, Zhou T, Wu H, Preparation and degradation of chitosan-poly(p-dioxanone)/silk fibroin porous conduits, Polymer Degradation and Stability 119 (2015) 46–55.

[62]. Wu H, Zhang J, Luo Y, Wan Y, Sun S, Mechanical properties and permeability of porous chitosan-poly(p-dioxanone)/silk fibroin conduits used for peripheral nerve repair, Journal of the Mechanical Behavior of Biomedical Materials 50 (2015) 192–205. [PubMed: 26143352]

[63]. Zhou Z, Liu X, Wu W, Park S, Miller AL II, Terzic A, Lu L, Effective nerve cell modulation by electrical stimulation of carbon nanotube embedded conductive polymeric scaffolds, Biomaterials Science 6(9) (2018) 2375–2385. [PubMed: 30019709]

[64]. Chi N, Wang R, Electrospun protein-CNT composite fibers and the application in fibroblast stimulation, Biochemical and Biophysical Research Communications 504(1) (2018) 211–217. [PubMed: 30172370]

[65]. Asadian M, Chan KV, Norouzi M, Grande S, Cools P, Morent R, De Geyter N, Fabrication and Plasma Modification of Nanofibrous Tissue Engineering Scaffolds, Nanomaterials 10(1) (2020).

[66]. Carvalho CR, Silva-Correia J, Oliveira JM, Reis RL, Nanotechnology in peripheral nerve repair and reconstruction, Advanced Drug Delivery Reviews 148 (2019) 308–343. [PubMed: 30639255]

[67]. Farzamfar S, Salehi M, Tavangar SM, Verdi J, Mansouri K, Ai A, Malekshahi ZV, Ai J, A novel polycaprolactone/carbon nanofiber composite as a conductive neural guidance channel: an in vitro and in vivo study, Progress in Biomaterials 8(4) (2019) 239–248. [PubMed: 31833033]

[68]. Uz M, Mallapragada SK, Conductive Polymers and Hydrogels for Neural Tissue Engineering, Journal of the Indian Institute of Science 99(3) (2019) 489–510.

[69]. Matsumoto K, Sato C, Naka Y, Whitby RLD, Shimizu N, Stimulation of neuronal neurite outgrowth using functionalized carbon nanotubes, Nanotechnology 21(11) (2010).

[70]. Matsumoto K, Shimizu N, Activation of the phospholipase C signaling pathway in nerve growth factor-treated neurons by carbon nanotubes, Biomaterials 34(24) (2013) 5988–5994. [PubMed: 23669261]

[71]. Yan L, Zhao B, Liu X, Li X, Zeng C, Shi H, Xu X, Lin T, Dai L, Liu Y, Aligned Nanofibers from Polypyrrole/Graphene as Electrodes for Regeneration of Optic Nerve via Electrical Stimulation, Acs Applied Materials & Interfaces 8(11) (2016) 6834–6840. [PubMed: 26926578]

[72]. Qian Y, Cheng Y, Cai J, Zhao X, Ouyang Y, Yuan W-E, Fan C, Advances in electrical and magnetic stimulation on nerve regeneration, Regenerative Medicine 14(10) (2019) 969–979. [PubMed: 31583954]

[73]. Uz M, Buyukoz M, Sharma AD, Sakaguchi DS, Altinkaya SA, Mallapragada SK, Gelatin-based 3D conduits for transdifferentiation of mesenchymal stem cells into Schwann cell-like phenotypes, Acta Biomaterialia 53 (2017) 293–306. [PubMed: 28213098]

[74]. Kang Y, Liu Y, Liu Z, Ren S, Xiong H, Chen J, Duscher D, Machens H-G, Liu W, Guo G, Zhan P, Chen H, Chen Z, Differentiated human adipose-derived stromal cells exhibit the phenotypic and functional characteristics of mature Schwann cells through a modified approach, Cytotherapy 21(9) (2019) 987–1003. [PubMed: 31351800]

[75]. Park H-W, Lim M-J, Jung H, Lee S-P, Paik K-S, Chang M-S, Human Mesenchymal Stem Cell-Derived Schwann Cell-Like Cells Exhibit Neurotrophic Effects, Via Distinct Growth Factor Production, in a Model of Spinal Cord Injury, Glia 58(9) (2010) 1118–1132. [PubMed: 20468053]

[76]. Sharma AD, Zbarska S, Petersen EM, Marti ME, Mallapragada SK, Sakaguchi DS, Oriented growth and transdifferentiation of mesenchymal stem cells towards a Schwann cell fate on micropatterned substrates, Journal of Bioscience and Bioengineering 121(3) (2016) 325–335. [PubMed: 26371993]

[77]. Das SR, Uz M, Ding S, Lentner MT, Hondred JA, Cargill AA, Sakaguchi DS, Mallapragada S, Claussen JC, Electrical Differentiation of Mesenchymal Stem Cells into Schwann-Cell-Like Phenotypes Using Inkjet-Printed Graphene Circuits, Advanced Healthcare Materials 6(7) (2017).

[78]. Uz M, Donta M, Mededovic M, Sakaguchi DS, Mallapragada SK, Development of Gelatin and Graphene-Based Nerve Regeneration Conduits Using Three-Dimensional (3D) Printing Strategies for Electrical Transdifferentiation of Mesenchymal Stem Cells, Industrial & Engineering Chemistry Research 58(18) (2019) 7421–7427.

[79]. Uz M, Hondred JA, Donta M, Jung J, Kozik E, Green J, Sandquist EJ, Sakaguchi DS, Claussen JC, Mallapragada S, Determination of Electrical Stimuli Parameters To Transdifferentiate Genetically Engineered Mesenchymal Stem Cells into Neuronal or Glial Lineages, Regenerative Engineering and Translational Medicine 6(1) (2020) 18–28.

[80]. Hu X, Wang X, Xu Y, Li L, Liu J, He Y, Zou Y, Yu L, Qiu X, Guo J, Electric Conductivity on Aligned Nanofibers Facilitates the Transdifferentiation of Mesenchymal Stem Cells into Schwann Cells and Regeneration of Injured Peripheral Nerve, Advanced Healthcare Materials 9(11) (2020).

[81]. Arslantunali D, Budak G, Hasirci V, Multiwalled CNT-pHEMA composite conduit for peripheral nerve repair, Journal of Biomedical Materials Research Part A 102(3) (2014) 828–841. [PubMed: 23554154]

[82]. Arthur-Farraj PJ, Latouche M, Wilton DK, Quintes S, Chabrol E, Banerjee A, Woodhoo A, Jenkins B, Rahman M, Turmaine M, c-Jun reprograms Schwann cells of injured nerves to generate a repair cell essential for regeneration, Neuron 75(4) (2012) 633–647. [PubMed: 22920255]

[83]. Liu X, Peng S, Zhao Y, Zhao T, Wang M, Luo L, Yang Y, Sun C, AMPK Negatively Regulates Peripheral Myelination via Activation of c-Jun, Molecular Neurobiology 54(5) (2017) 3554–3564. [PubMed: 27194296]

[84]. Yuk H, Lu B, Zhao X, Hydrogel bioelectronics, Chemical Society Reviews 48 (2019) 1642–1667. [PubMed: 30474663]

[85]. Zhao S, Tseng P, Grasman J, Wang Y, Li W, Napier B, Yavuz B, Chen Y, Howell L, Rincon J, Omenetto FG, Kaplan DL, Programmable hydrogel ionic circuits for biologically matched electronic interfaces, Advanced Materials 30 (2018) 1800598.

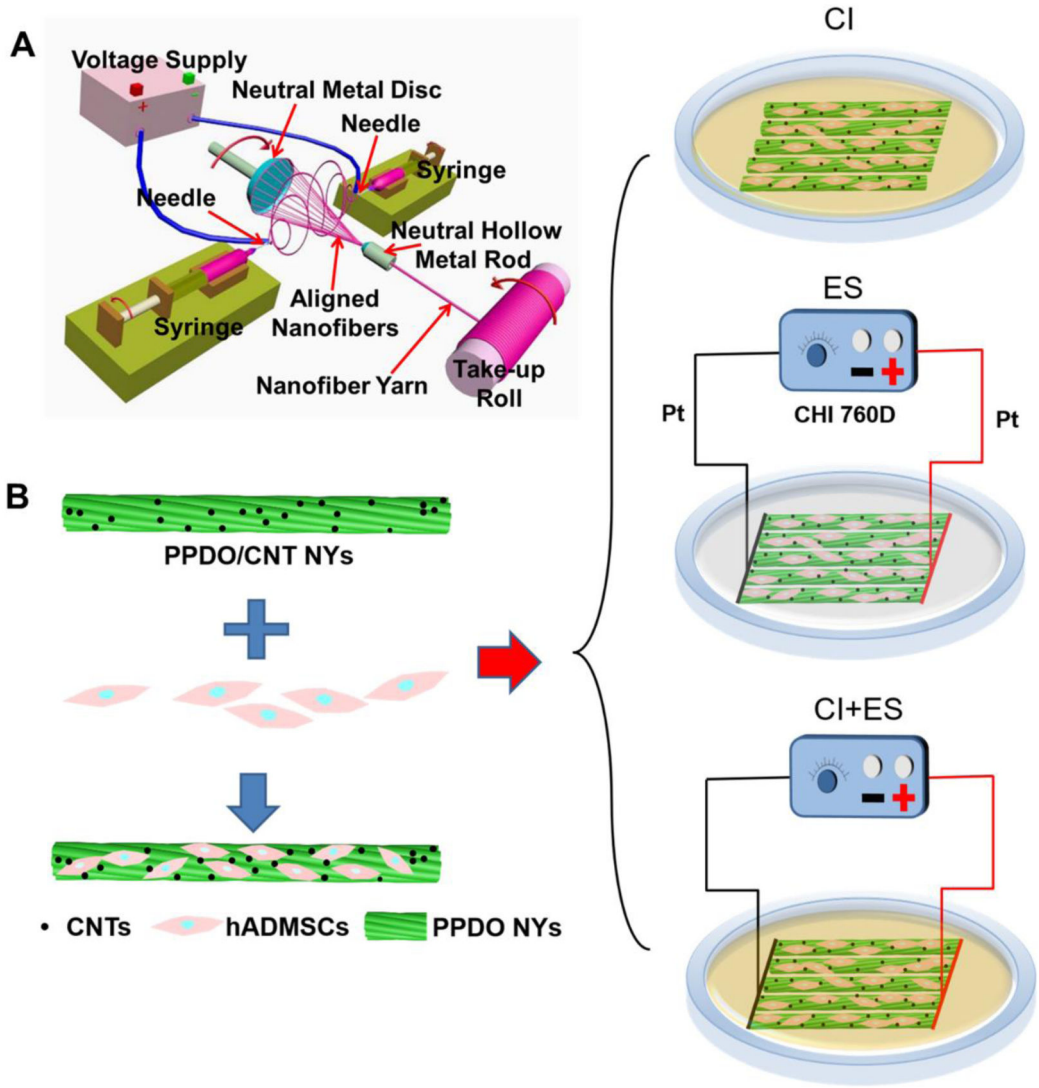

Figure 1.

(A) Schematic of our electrospun nanofiber yarn-forming device and nanofiber yarn fabrication. (B) Experimental design of hADMSCs differentiation towards SCLCs by using CI, ES, and their combination.

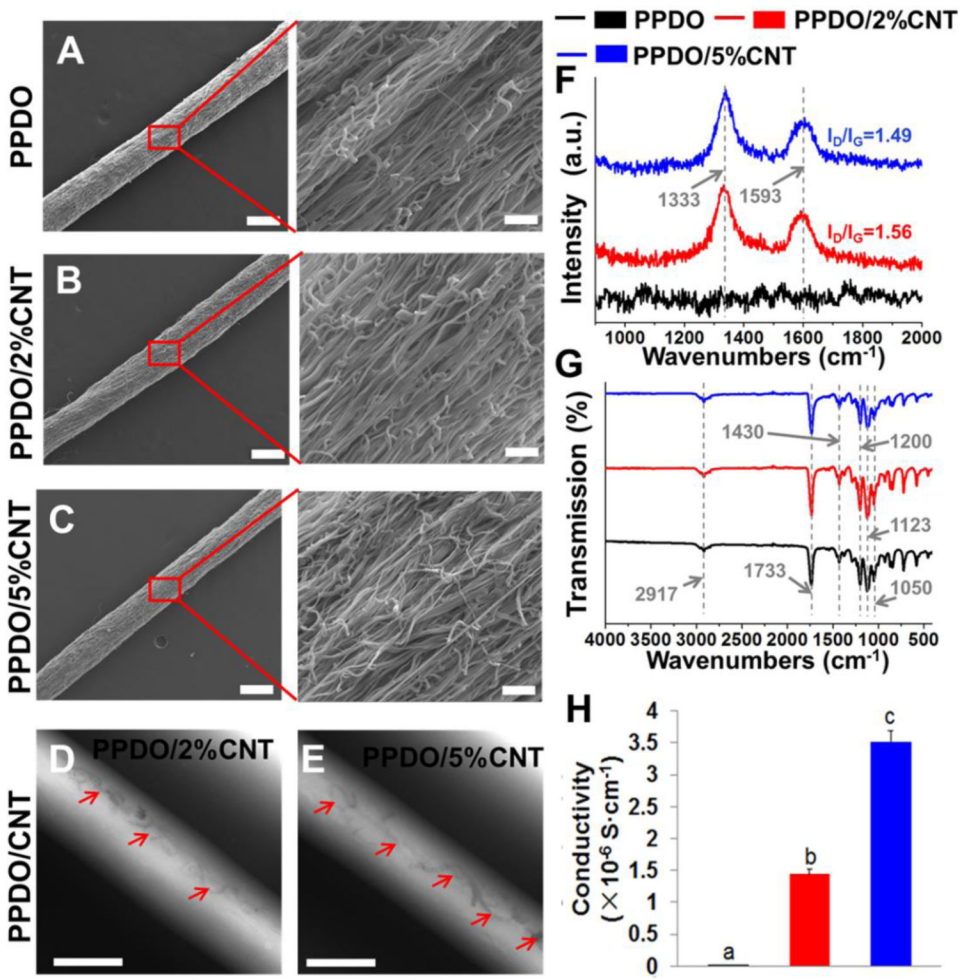

Figure 2.

SEM images of three different NY materials: (A) PPDO NYs; (B) PPDO/2%CNT NYs; (C) PPDO/5%CNT NYs; Scale bar: 200 μm for left panel and 20 μm for right panel. TEM images of PPDO/CNT nanofibers: (D) PPDO/2%CNT nanofibers; (E) PPDO/5%CNT nanofibers; Scale bar=500 nm; The red arrows show the positions of CNTs. (F) Raman spectra of PPDO NYs, PPDO/2%CNT NYs, and PPDO/5%CNT NYs; (G) FTIR spectra of PPDO NYs and two types of PPDO/CNT NYs; (H) Electrical conductivity of three different as-obtained NY materials, without or with CNTs (n=5; bars with different letters represent a significant difference between two groups, p<0.01).

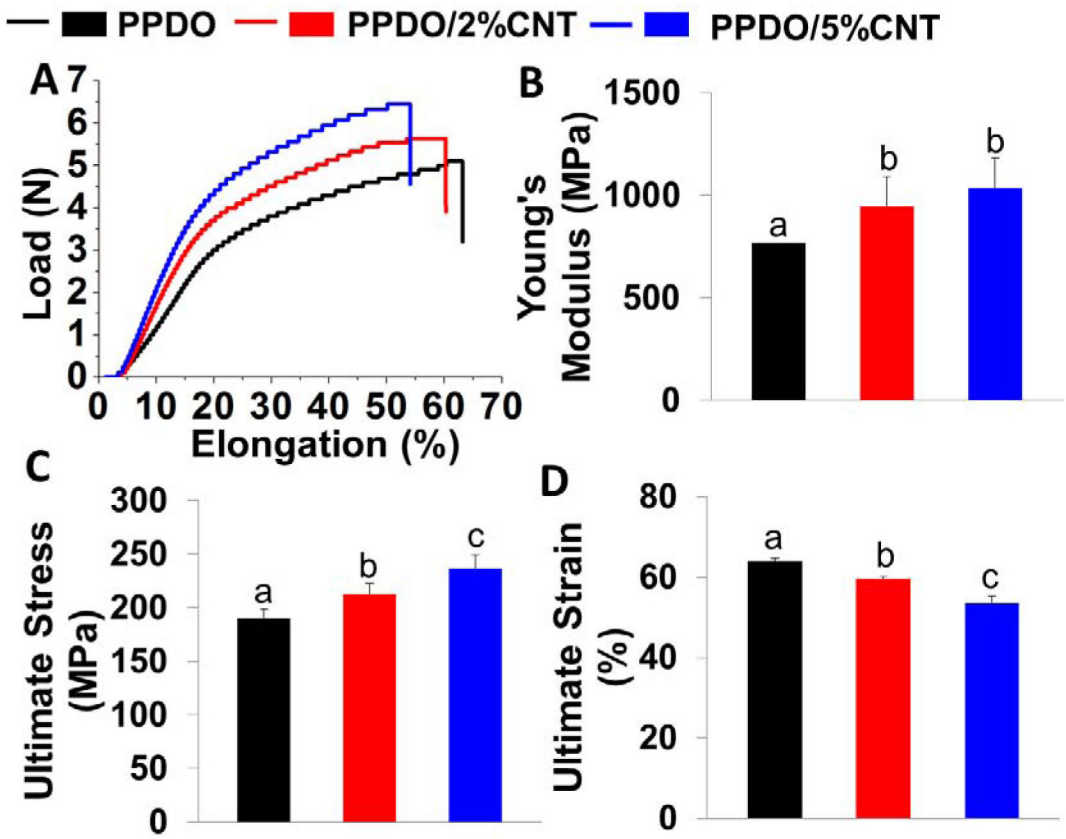

Figure 3.

Mechanical properties of PPDO NYs, PPDO/2%CNT NYs, and PPDO/5%CNT NYs: (A) Typical load-elongation curves; (B) Young's modulus; (C) Ultimate strength; (D) Ultimate strain (n=5; bars with different letters represent a significant difference between two groups, $p<0.05$).

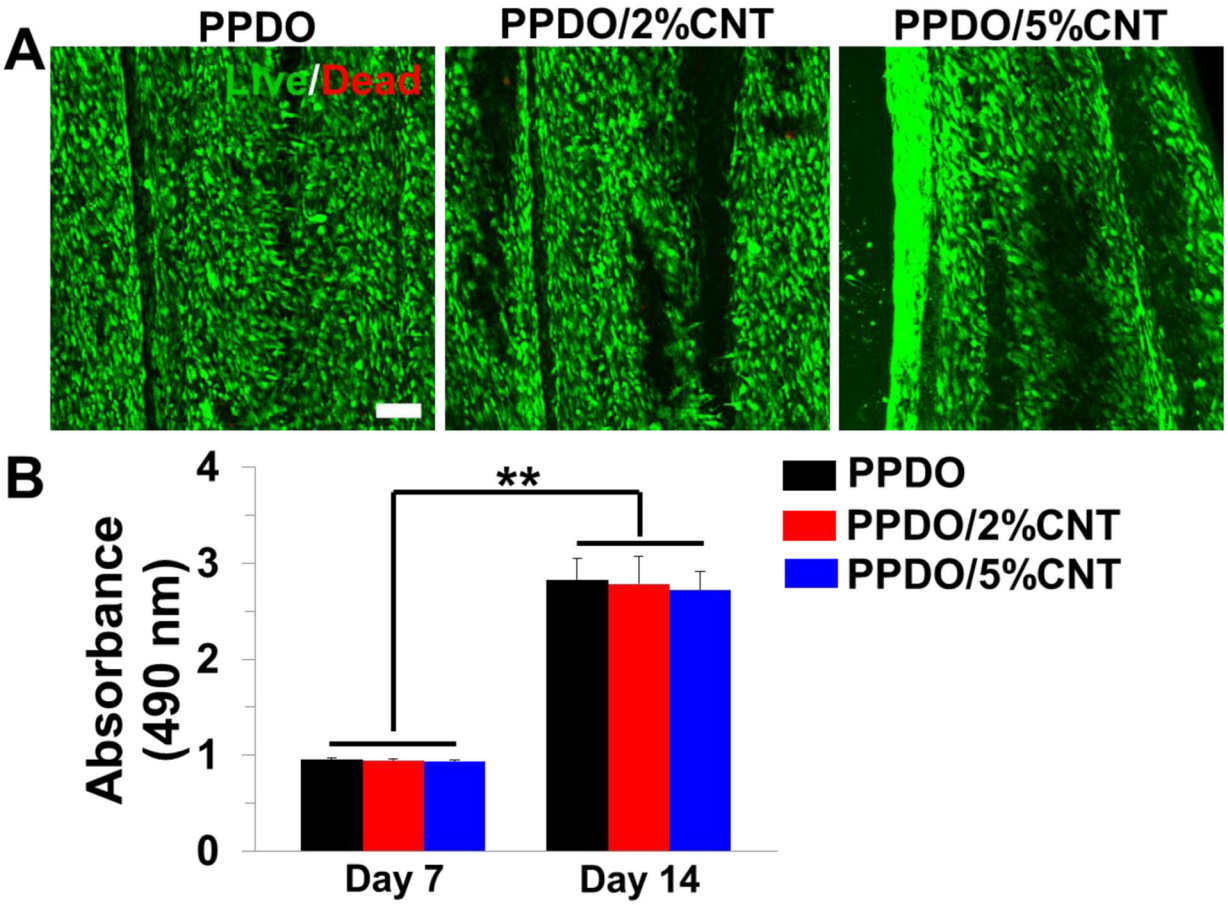

Figure 4.

(A) Representative images of Live/Dead staining of rSCs seeded on PPDO NYs, PPDO/2%CNT NYs, and PPDO/5%CNT NYs throughout 14 days of culture; Scale bar=100μm. (B) MTT analysis of rSCs seeded on PPDO NYs, PPDO/2%CNT NYs, and PPDO/5%CNT NYs for 14 days of culture (n=5; ** represent a significant difference between two groups, $p<0.01$).

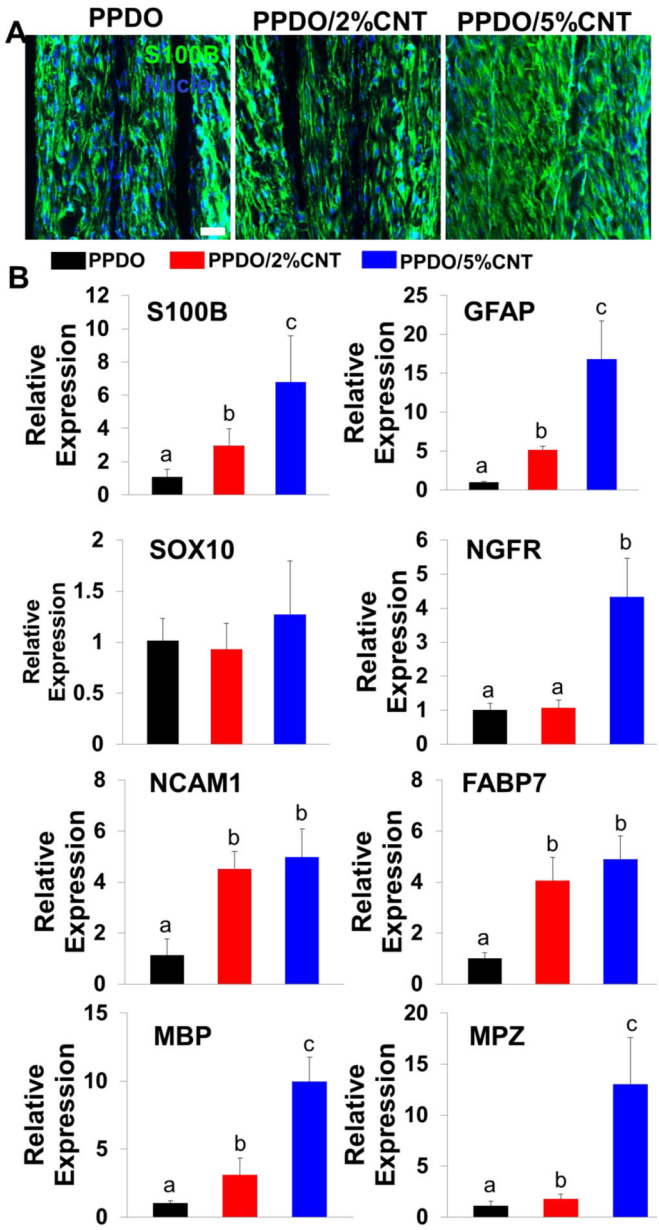

Figure 5.

(A) IF staining for S100B (green), and nuclei (blue) of rSCs on PPDO NYs, PPDO/2%CNT NYs and PPDO/5%CNT NYs after 14 days of culture; Scale bar=50 μm. (B) QRT-PCR analysis of S100B, GFAP, SOX10, NGFR, NCAM1, FABP7, MBP, and MPZ mRNA expression of rSCs seeded on three different NY materials after 14 days of culture. Relative expression is presented as normalized to 18S mRNA and relative to rSCs seeded on PPDO NY bundles (n=3; bars with different letters represent a significant difference between two groups, $p<0.05$).

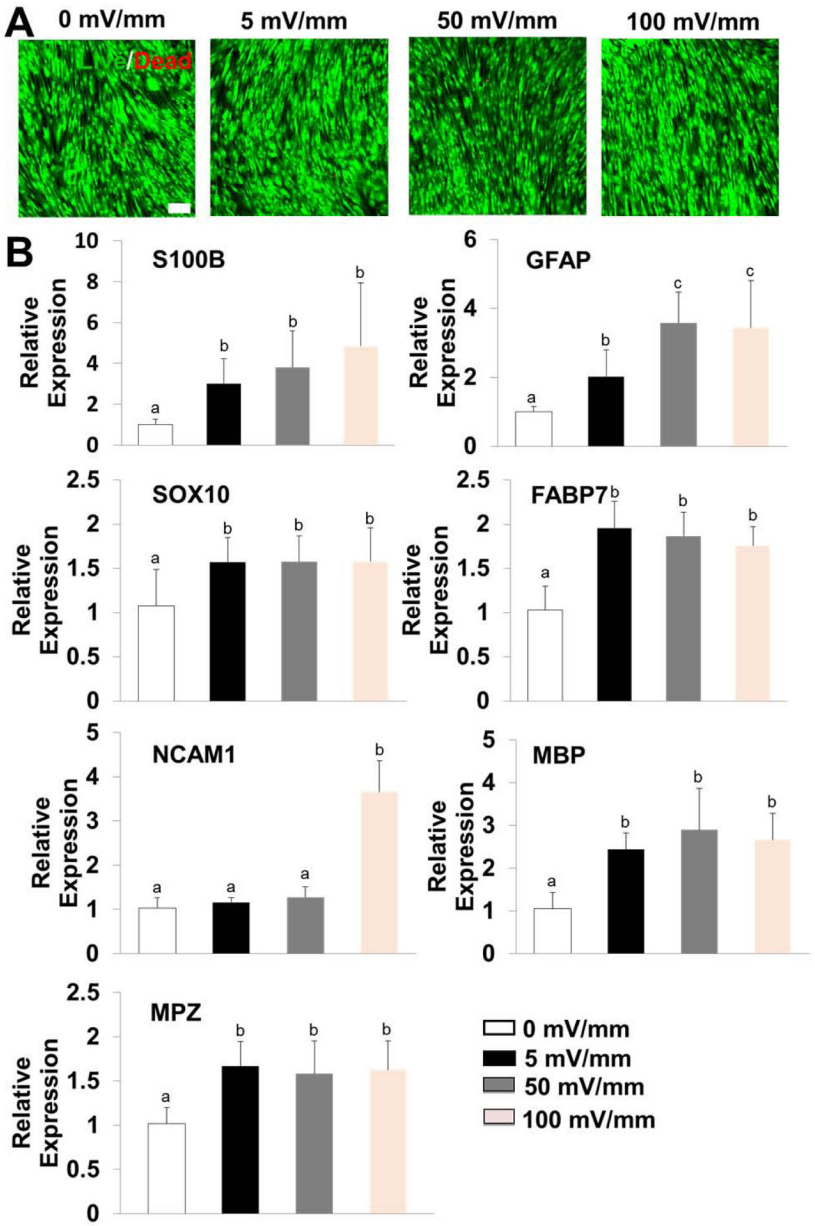

Figure 6.

(A) Representative images of Live/Dead staining of rSCs seeded on 2D substrates under ES treatment with different potentials ranging from 0–100 mV/mm throughout 7 days of culture; Scale bar=100μm. (B) QRT-PCR analysis of S100B, GFAP, SOX10, NCAM1, FABP7, MBP, and MPZ mRNA expression of rSCs seeded on glass substrates under ES treatment with different potentials ranging from 0–100 mV/mm throughout 7 days of culture. Relative expression is presented as normalized to 18S mRNA and relative to rSCs seeded on glass substrates and unstimulated (n=3; bars with different letters represent a significant difference between two groups, $p<0.05$).

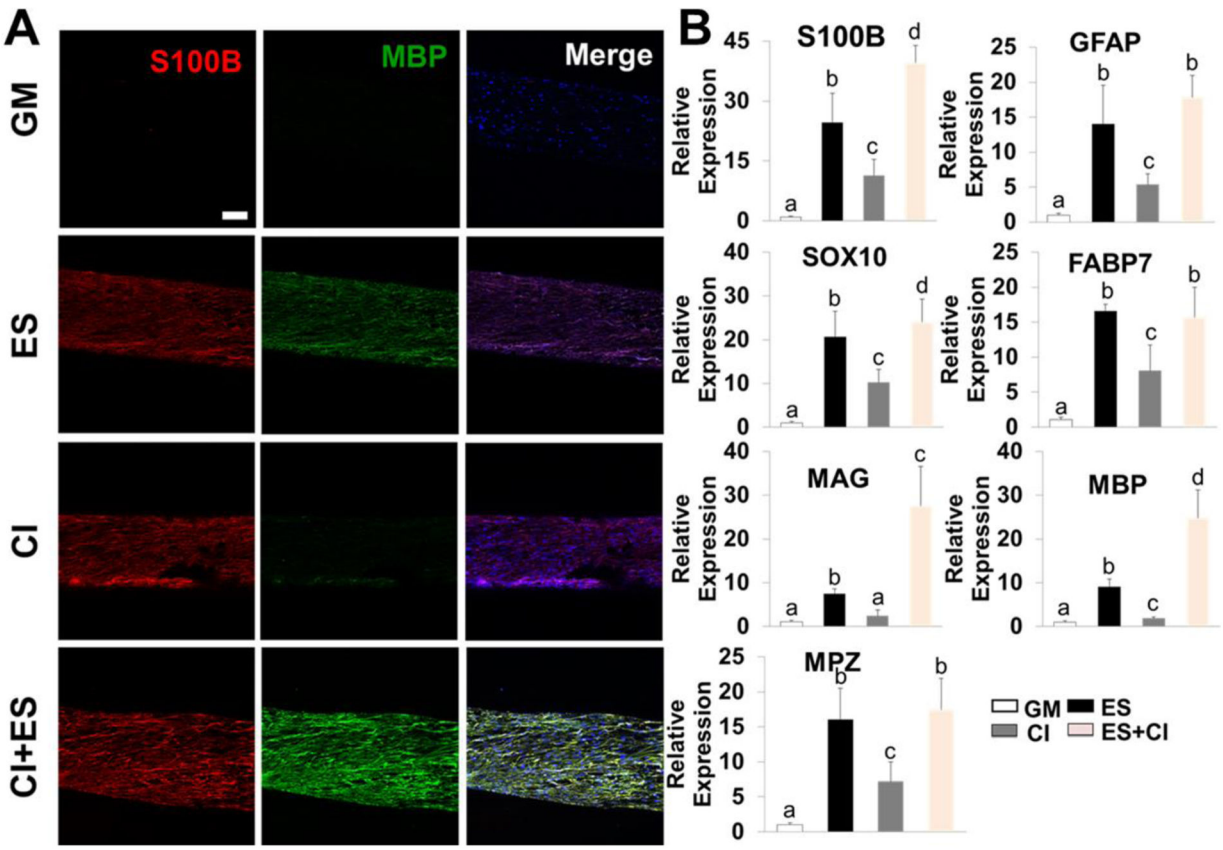

Figure 7.

(A) IF staining for S100B (red), MBP (green), and nuclei (blue) of hADMSCs seeded on PPDO/5%CNT NYs with different treatments, including GM, ES, CI, and a combination of ES and CI throughout, 14 days of culture; Scale bar=100 μm. (B) QRT-PCR analysis of S100B, GFAP, SOX10, FABP7, MBP, and MPZ mRNA expression of hADMSCs seeded on PPDO/5%CNT NYs with different treatments, including GM, ES, CI, and a combination of ES and CI, throughout 14 days of culture. Relative expression is presented as normalized to 18S mRNA and relative to hADMSCs seeded on PPDO/5%CNT NYs and cultured in GM (n=3; bars with different letters represent a significant difference between two groups, $p<0.05$).

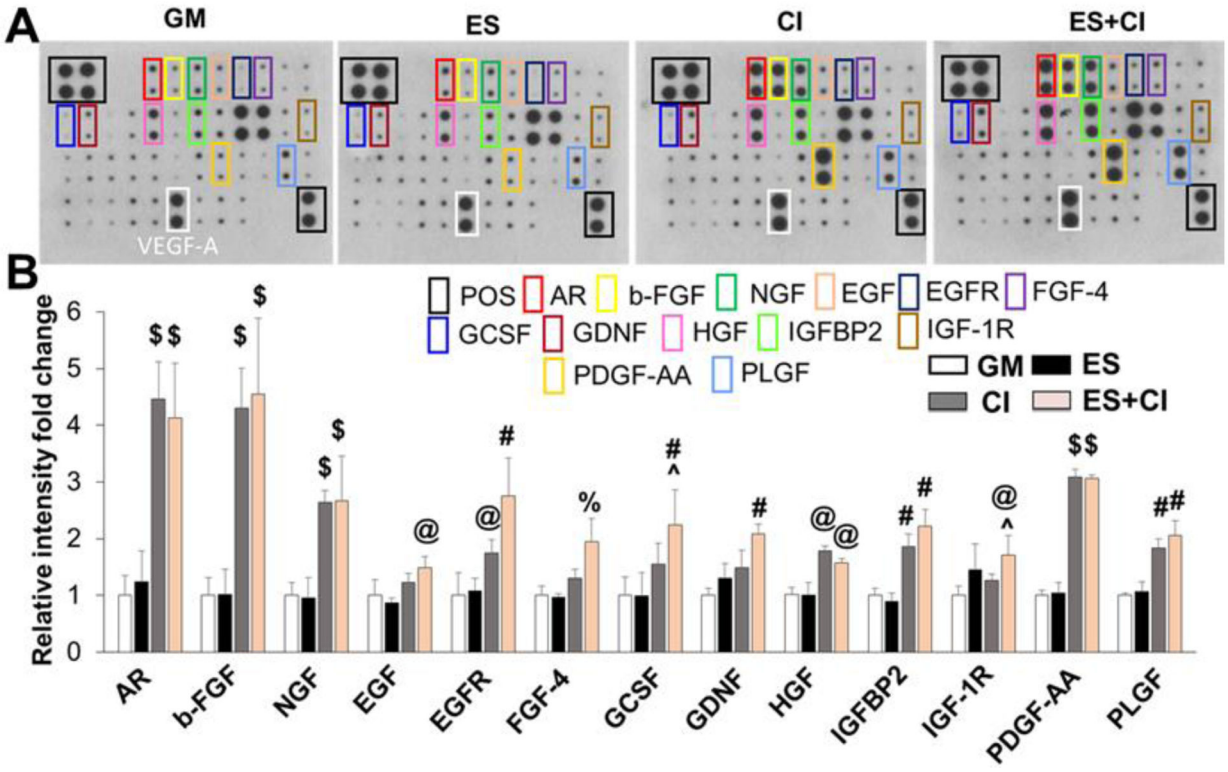

Figure 8.

Secretion of growth factors from hADMSC-SCLCs in GM, ES, CI, and ES+CI groups. (A) Representative images of human growth factor array assay. (B) Semi-quantitative analysis of the secreted growth factors with statistical difference. Relative expression of each targeted growth factor was presented as normalized to the positive control on the same array and relative to hADMSC-SCLCs in GM group (n=4; @ $p<0.05$ compared to GM and ES groups, #$p<0.01$ compared to GM and ES groups, $ $p<0.001$ compared to GM and ES groups, % $p<0.05$ compared to GM, ES, and CI groups, ^ $p<0.05$ compared to CI group).